J. Plasma Physics (2000), *vol.* 63, *part* 5, *pp.* 495–510. Printed in the United Kingdom

© 2000 Cambridge University Press

Instabilities in localized non-uniform charged dust streams in cold plasmas

VLADIMIR M. ČADEŽ and FRANK VERHEEST
Sterrenkundig Observatorium, Universiteit Gent, Krijgslaan 281, B-9000 Gent, Belgium

(Received 23 October 1999)

Abstract. Surface eigenmodes in a dusty plasma, where the dust is confined to a particular region, modelled as a uniform slab with non-uniform smooth boundary layers, are discussed. Inside this region, electron depletion occurs, while outside it, the plasma is just a normal uncontaminated plasma. In addition, the dust component can flow with respect to the background plasma, as a first approximation to cometary tails, where there is a notable difference between the fast flowing solar wind and the slow moving dust tail, viewed in the comet frame. The equilibrium densities and flow are non-uniform and the description involves a space-dependent dielectric function, which indicates the possibility of singular points, where eigenmodes resonate with local plasma oscillations. Surface eigenmodes on the slab are obtained analytically in the limit of long wavelengths, and these give rise to two distinct frequency domains, both having three different wave solutions. One of these refers to plasma surface waves, unaffected by the dust flow. The other two lead to convective surface modes, which become unstable for large flow speeds, akin to Buneman-type instabilities. A detailed study is made of the resonant processes in the boundary layers, including damping and growth rates.

1. Introduction

The presence of charged dust in a plasma environment has recently emerged as a novel and radically different area of plasma physics, potentially of great importance because dust and plasmas are ubiquitous in space and astrophysics. Although it had been known for a long time that dust grains immersed in a plasma and radiative environment would pick electrons and to a lesser extent ions from their surroundings (Spitzer 1941), it took the space age to confront us with phenomena such as the spokes and braids in the rings of Saturn that could not be satisfactorily explained by ordinary gravitodynamical theories (Bliokh and Yaroshenko 1985). Since then, the subject has been developing at a rapid pace, so that the theoretical developments have largely outstripped the too scarce (indirect) observational evidence. Several review papers (Shukla 1992; Mendis and Rosenberg 1994; Horányi 1996; Verheest 1996) and a monograph (Bliokh et al. 1995) have been written about different aspects of these dusty plasmas in space, and we refer to these for further details, especially about the great variety of modified plasma and novel dust wave modes. There is now also a welcome complement of knowledge flowing from various ingenious experiments, where the charged dust grains can be seen with the naked eye, but these fall outside the scope of the present paper.

https://doi.org/10.1017/S0022377800008333 Published online by Cambridge University Press

Many of the theoretical wave modes have been developed for infinite and homogeneous plasmas, or in media with slowly varying characteristics, but space plasmas are bounded and separated from surrounding regions by boundary layers. Typical examples are cometary tails downstream from the nucleus, or the plasma torus emanating from Io in the Jovian magnetosphere, or when highly structured flux tubes occur owing to the presence of an external magnetic field. Surprisingly enough, surface waves on these boundaries of a dusty plasma have not been studied in great detail.

Bharuthram and Shukla (1993) deal with low-frequency surface waves in a plasma with warm electrons and ions, in addition to cold dust, and occupying a half-space with a sharp vacuum–plasma interface. The surface dust-acoustic mode thus derived goes over in the long-wavelength limit to the volume dust-acoustic mode (Rao et al. 1990). In these modes, the electron and ion pressures provide the tension and the much heavier dust the inertia to maintain the wave. A possible application is to interstellar clouds, if there is a sharp boundary between vacuum and expanding plasma. This treatment was later generalized by Kotsarenko et al. (1998) to external magnetic field effects, in both plane and cylindrical geometries. The low-frequency motion of the dust grains, between the dust cyclotron and plasma frequencies, has been studied in two regimes. One type of waves propagate along the magnetic field, if it is parallel to the boundary delineating the plasma region, with velocities smaller than the volume dust-acoustic velocity. When the magnetic field is perpendicular to the surface, surface waves with higher phase velocities are possible. Wavelike structures in cometary plasma tails have been considered, where wavelengths of several thousand kilometres have been observed. Good agreement with theory is claimed for average parameters. Several papers have addressed low-frequency Alfvén surface waves in a structured magnetized dusty plasma, characterized either by sharp interfaces between dusty plasma and vacuum or dielectric regions (Ostrikov and Yu 1998; Ostrikov et al. 1999) or by rather narrow but smooth transitions between dusty plasma and vacuum (Cramer and Vladimirov 1996; Cramer et al. 1998).

In this paper, we discuss surface eigenmodes in a different dusty plasma model. Since plasmas pervade larger regions than dust, as in cometary tails, which are surrounded by the solar wind plasma, we shall assume that the dust is confined to a particular region and that electron attachment occurs inside this region. Outside, the plasma is just a normal uncontaminated plasma. In order to point out the salient features of this model, we use in this paper a dust slab or layer for simplicity, without external magnetic field, but for which the boundary layers have a certain width. The presence of dust reduces the electron concentration inside the layer, but we shall assume the ions to have constant density throughout. In addition, the dust component can flow with respect to the plasma, as a first approximation to cometary tails, where there is a notable difference between the fast flowing solar wind and the slow moving dust tail, viewed in the comet frame.

The paper is structured as follows. In Sec. 2, we discuss the basic state assumptions, and then set up in Sec. 3 the equations describing linear perturbations of the chosen model. Since the equilibrium densities and flows are non-uniform, the description yields a space-dependent dielectric function, for

https://doi.org/10.1017/S0022377800008333 Published online by Cambridge University Press

wave modes propagating inside the dust layer. Since this dielectric function indicates the existence of singular points, resonances are possible with local plasma oscillations. In Sec. 4, we then study eigenmodes that are evanescent outside the dust layer, and use standard electromagnetic boundary conditions to match the solutions from the uniform inside and outside regions through the boundary layers on both sides of the dusty plasma region. If the latter are sufficiently sharp, we obtain approximate solutions, and these lead in Sec. 5 to the dispersion law. The analysis of the possible frequency spectra in Sec. 6 indicates two distinct domains, each of which has pairs of solutions. One of these refers to plasma surface waves, unaffected by the dust flow. The other pair refers to convective surface modes, which become unstable for large flow speeds, akin to Buneman-type instabilities. Section 7 is devoted to a more detailed study of the resonant processes in the boundary layers, including damping and growth rates, which are given in Sec. 8. Finally, Sec. 9 contains our conclusions.

2. Basic state assumptions

We consider a plasma composed of electrons (e), ions (i) and dust (d) particles with respective equilibrium concentrations $N_{e,i,d}(x)$. In what follows, the ions are taken to be ionized hydrogen atoms, i.e. protons, while the dust particles are assumed to be negatively charged by the attachment of electrons. The presence of dust thus reduces the concentration of electrons but leaves the ion density unaffected.

The whole plasma system is assumed to be electrically neutral in the basic unperturbed state, so that

$$N_i(x) = Z_d N_d(x) + N_e(x)$$

for an electron–proton–dust plasma with Z_d electrons attached to each dust particle. Here $\alpha \equiv e, i, d$ and the particle charges are as follows: $q_e = -e$, $q_i = e$ and $q_d = -Z_d e$, while the masses are ordered as $m_d \gg m_i \gg m_e$. The dust component is assumed to be localized to a layer and to move with a flow velocity $\mathbf{U}_d = U_d(x)\,\mathbf{e}_y$ through a static and fully ionized electron–hydrogen plasma background. Plasma parameters are constant in the major part of this layer (region 1), where $x \in (-x_0, +x_0)$, and they vary continuously but rather steeply with x through transitional boundary layers of thickness $\Delta \ll x_0$ at each side of the dusty plasma flow. Outside the layer (region 2), for $x \geqslant x_0 + \Delta$ and $x \leqslant -x_0 - \Delta$, there is no dust, and the medium is a uniform stationary plasma composed of electrons and protons only. The configuration is illustrated in Fig. 1.

The electron densities N_{e1} and N_{e2} in regions 1 and 2 differ from each other, while the density of ions $N_i(x)$ is taken to be constant throughout the whole space, including the boundary layers: $N_i(x) = \text{const}$ or $N_{i1} = N_{i2} \equiv N_i$. As to the moving dust component, we have $N_{d1} = 0$ and $N_{2d} \neq 0$, with the dust flow speed $U_d(x)$ varying across the boundary layer from 0 in region 1 to $U_2 = \text{const}$ in region 2.

https://doi.org/10.1017/S0022377800008333 Published online by Cambridge University Press

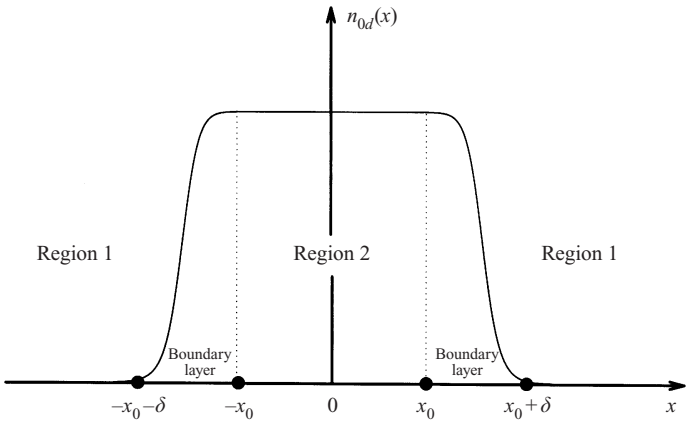


Figure 1. Schematic density profile of the dust component.

3. Governing equations for linear perturbations

This basic state is subject to linear harmonic perturbations, and we shall restrict ourselves to disturbances that are unaffected by thermal motions, i.e. all three plasma components are considered as effectively cold. The linearized equations governing such perturbations consist of the continuity equations for each species

$$\frac{\partial n_\alpha}{\partial t}+N_\alpha \nabla\cdot\mathbf{v}_\alpha+\mathbf{v}_\alpha\cdot\nabla N_\alpha+\mathbf{U}_\alpha\cdot\nabla n_\alpha=0,$$

and the momentum equations

$$\frac{\partial \mathbf{v}_\alpha}{\partial t}+(\mathbf{v}_\alpha\cdot\nabla)\,\mathbf{U}_\alpha+(\mathbf{U}_\alpha\cdot\nabla)\,\mathbf{v}_\alpha=\frac{q_\alpha}{m_\alpha}\mathbf{E}.$$

The flow velocity $\mathbf{U}_\alpha$ only exists for the dust component, i.e. $\mathbf{U}_{i,e}\equiv 0$ and $\mathbf{U}_d(x)\equiv\mathbf{U}(x)$. The set is closed by Gauss's law

$$\nabla\cdot\mathbf{E}=\frac{1}{\epsilon_0}\sum_\alpha q_\alpha n_\alpha.$$

Any perturbed quantity ψ will be taken to be harmonic in time t and two spatial coordinates y and z, but its amplitude remains a function of x:

$$\psi=\psi(x)\exp(-i\omega t+i\mathbf{k}_\parallel\cdot\mathbf{r}),\qquad\text{with}\quad \mathbf{k}_\parallel\equiv(0,k_y,k_z).$$

With this Fourier transformation with respect to the variables t, y and z, the model equations become

$$-i\tilde{\omega}_\alpha\mathbf{v}_\alpha+v_{\alpha x}\frac{dU_\alpha}{dx}\mathbf{e}_y=\frac{q_\alpha}{m_\alpha}\mathbf{E},\tag{1}$$

$$i\tilde{\omega}_\alpha n_\alpha=N_\alpha\left(\nabla\cdot\mathbf{v}_\alpha+\frac{d\ln\omega_{p\alpha}^2}{dx}v_{\alpha x}\right),\tag{2}$$

$$i\mathbf{k}_\parallel\cdot\mathbf{E}+\frac{dE_x}{dx}=\frac{1}{\epsilon_0}\sum_\alpha n_\alpha q_\alpha,\tag{3}$$

https://doi.org/10.1017/S0022377800008333 Published online by Cambridge University Press

with

$$\tilde{\omega}_\alpha \equiv \omega - k_\parallel U_\alpha(x),$$

$$\omega_{p\alpha} = \omega_{p\alpha}(x) \equiv \left(\frac{N_\alpha q_\alpha^2}{\epsilon_0 m_\alpha}\right)^{1/2}$$

being the local Doppler-shifted wave frequency and the plasma frequency respectively, for the species α.

Equations (1) and (2) now yield

$$\mathbf{v}_\alpha = i\frac{q_\alpha}{m_\alpha \tilde{\omega}_\alpha}\mathbf{E} + \frac{q_\alpha E_x}{m_\alpha \tilde{\omega}_\alpha^2}\frac{dU_\alpha}{dx}\mathbf{e}_y,$$

$$n_\alpha = \frac{\epsilon_0}{q_\alpha}\boldsymbol{\nabla}\cdot\left(\mathbf{E}\frac{\omega_{p\alpha}^2}{\tilde{\omega}_\alpha^2}\right),$$

where the relations

$$\frac{d\tilde{\omega}_\alpha}{dx} = -k_y\frac{dU_\alpha}{dx},$$

$$\boldsymbol{\nabla} = i\mathbf{k}_\parallel + \frac{d}{dx}\mathbf{e}_x$$

have been taken into account.

Equation (3) thus reduces to

$$\frac{d}{dx}[\epsilon(x;\omega)\,E_x] + i\epsilon(x;\omega)\,\mathbf{k}_\parallel\cdot\mathbf{E} = 0, \tag{4}$$

with the relative dielectric function $\epsilon(x;\omega)$ given by

$$\epsilon(x;\omega) \equiv 1 - \frac{\omega_{pe}^2(x)}{\omega^2} - \frac{\omega_{pi}^2}{\omega^2} - \frac{\omega_{pd}^2(x)}{\tilde{\omega}_d^2(x)}. \tag{5}$$

Introducing the electric potential ϕ through $\mathbf{E} = -\boldsymbol{\nabla}\phi$, (4) can be expressed in the following way:

$$\frac{d}{dx}\left[\epsilon(x;\omega)\frac{d\phi}{dx}\right] - k_\parallel^2\,\epsilon(x;\omega)\,\phi = 0. \tag{6}$$

Equation (6) is singular, with poles at points $x = x_r$, where $\epsilon(x_r;\omega)$ vanishes:

$$\frac{\omega_{pe}^2(x_r)}{\omega^2} + \frac{\omega_{pi}^2}{\omega^2} + \frac{\omega_{pd}^2(x_r)}{\tilde{\omega}_d^2(x_r)} = 1. \tag{7}$$

The divergence of the potential and its x derivative at $x = x_r$ arises owing to the initial assumption in our model of the plasma being without dissipation. Consequently, (6) cannot be fully applied in the vicinity of singular points and its solutions have to be locally modified by including some dissipation.

The existence of singular points indicates the possibility for a harmonic wave to resonantly interact with local plasma oscillations at $x = x_r$ and whose dispersion relation is $\epsilon(x_r;\omega_0) = 0$.

4. Boundary conditions and solutions

We shall study linear surface eigenmodes attached to the described plasma layer configuration with charged dust particles moving in it. The eigenmode solutions of (6) for which we are looking are evanescent outside the layer and

https://doi.org/10.1017/S0022377800008333 Published online by Cambridge University Press

obey two standard boundary conditions that require continuity of both the electric potential ϕ and of the x component of the electric displacement vector $D_x = \epsilon_0 \epsilon(x;\omega) E_x$. The electric permittivity of free space is ϵ_0, but we shall take it to be equal to unity in further expressions in order to simplify the notation. The two boundary conditions are then

$$[\phi] = 0, \tag{8a}$$

$$[D_x] \equiv -\left[\epsilon \frac{d\phi}{dx}\right] = 0, \tag{8b}$$

and will be applied to the solutions at the four boundary points:

$$x = \pm x_0, \qquad x = \pm (x_0 + \Delta).$$

4.1. Solutions in uniform regions

The evanescent surface-wave solutions of (6) in the uniform domain outside the dust layer (region 1) are readily found to be

$$\phi^{(1)} = \begin{cases} C_1^{(+)} e^{k_\parallel x} & \text{for } x \leqslant -x_0 - \Delta, \\ C_1^{(-)} e^{-k_\parallel x} & \text{for } x_0 + \Delta \leqslant x, \end{cases} \tag{9}$$

while those in the uniform domain inside the layer (region 2) are

$$\phi^{(2)} = C_2^{(+)} e^{k_\parallel x} + C_2^{(-)} e^{-k_\parallel x} \quad \text{for } -x_0 \leqslant x \leqslant x_0. \tag{10}$$

The boundary conditions (8) will be used to determine the integration constants $C_{1,2}^{(+,-)}$ in the solutions (9) and (10) and also to connect these solutions through the non-uniform boundary layers of thickness Δ.

4.2. Approximate solutions in boundary layers

Solutions for ϕ in the two non-uniform boundary layers can only be obtained numerically, by solving (6) with prescribed basic state profiles entering the expression for $\epsilon(x;\omega)$. However, analytical solutions of (6) can be derived if we restrict our study to waves with comparatively long wavelengths, so that $k_\parallel \Delta \ll 1$. Taking $k_\parallel \Delta$ as a small parameter, (6) can be integrated through each of the two boundary layers. This enables us to connect the solutions (9) and (10) by computing only the changes or jumps of the potential ϕ across the two identical boundary layers of thickness Δ.

The first integration of (6) shows that the x component of the electrical displacement vector D_x remains constant across the layer, up to small terms $\mathcal{O}(k_\parallel \Delta)$, i.e.

$$D_x^{(n)} \equiv -\epsilon(x;\omega) \frac{d\phi^{(n)}}{dx} = \text{const} + \mathcal{O}(k_\parallel \Delta). \tag{11}$$

Here $n = 1, 2$ designate the boundary layers located at $x = -x_0$ and $x = +x_0$ respectively. Using the boundary conditions (8), we may write

$$D_x^{(n)} = -\epsilon_n \left.\frac{d\phi^{(n)}}{dx}\right|_{x=x_n},$$

where ϵ_n is the value of ϵ in the uniform regions 1 and 2 respectively, while x_n designates the left boundary point of each boundary layer: $x_1 = -(x_0 + \Delta)$ and

https://doi.org/10.1017/S0022377800008333 Published online by Cambridge University Press

$x_2 = x_0$. Finally, the jump condition for $D_x^{(n)}$ across the layer of thickness Δ is then simply

$$[D_x^{(n)}]_\Delta = 0.$$

A repeated integration of (11) gives an expression for the change of the potential ϕ across the layer. Here we have to take into account the singularities at $x = x_r$, which is done by including a weak dissipation through a small imaginary part $|\Gamma| \ll \omega$ added to the frequency. We therefore replace ω by $\omega + i\Gamma$, which then makes $\epsilon(x;\omega)$ complex, $\epsilon = \Re(\epsilon) + i\Im(\epsilon)$. Explicit expressions for $\Im(\epsilon)$ and $\Re(\epsilon)$ can be obtained by a Taylor expansion of ϵ in Γ as follows:

$$\epsilon(x;\omega+i\Gamma) = \epsilon(x;\omega) + i\Gamma \frac{\partial \epsilon(x;\omega+i\Gamma)}{\partial \omega}\bigg|_{\Gamma=0} + \mathcal{O}\left(\frac{\Gamma^2}{\omega^2}\right). \tag{12}$$

According to (4) and (12), the real and imaginary parts of ϵ are

$$\Re(\epsilon) = \epsilon(x;\omega), \tag{13a}$$

$$\Im(\epsilon) = 2\Gamma\left[\frac{\omega_{pe}^2(x)}{\omega^3} + \frac{\omega_{pi}^2}{\omega^3} + \frac{\omega_{pd}^2(x)}{\tilde{\omega}_d^3(x)}\right]. \tag{13b}$$

The imaginary part $\Im\epsilon$ thus becomes important only at singular points $x = x_r$ where $\Re\epsilon = 0$; otherwise it can be neglected as a small quantity with respect to $\Re\epsilon$. For this reason, we may write

$$\begin{aligned}\frac{1}{\epsilon(x;\omega)} &= \frac{\Re\epsilon}{(\Re\epsilon)^2 + (\Im\epsilon)^2} - i\frac{\Im\epsilon}{(\Re\epsilon)^2 + (\Im\epsilon)^2} \\ &= \frac{\Re\epsilon}{(\Re\epsilon)^2 + (\Im\epsilon)^2} - i\pi \sum_{x_r} \operatorname{sgn} \Im\epsilon(x;\omega) \left|\frac{d\epsilon}{dx}\right|^{-1} \delta(x - x_r),\end{aligned}$$

where $\delta(x - x_r)$ is the Dirac delta function and the summation is performed over all singularities, i.e. the resonant points x_r are the solutions of $\Re\epsilon(x_r;\omega_0) = 0$.

Equation (11) can now be integrated over x, yielding the jump condition for ϕ across the boundary layer of the following form:

$$[\phi]_\Delta = \Re[\phi]_\Delta + i\Im[\phi]_\Delta, \tag{14}$$

where

$$\Re[\phi]_\Delta = \mathcal{O}(k_\parallel \Delta), \tag{15a}$$

$$\Im[\phi]_\Delta = \pi D_x^{(n)} \Delta \sum_{x_r} \operatorname{sgn} \Im\epsilon(x_r;\omega_0) \left|\frac{\Delta \partial \epsilon}{\partial x}\right|^{-1}_{x=x_r} = \mathcal{O}(k_\parallel \Delta), \tag{15b}$$

since

$$\frac{1}{\epsilon}\left|\frac{\partial \epsilon}{\partial x}\right| \Delta = \mathcal{O}(1), \qquad D_x^{(n)} \Delta = \mathcal{O}(k_\parallel \Delta).$$

The change of ϕ thus obtained is a small complex quantity, with both real and imaginary parts being $\mathcal{O}(k_\parallel \Delta) \ll 1$, as seen in (15). The real part of the jump (15) causes only a small shift of the real part of the eigenfrequency, and for this reason it will be ignored in our study. The small imaginary part, however, will be crucial for wave damping and instabilities, since it introduces a small imaginary eigenfrequency shift $\mathcal{O}(k_\parallel \Delta)$.

https://doi.org/10.1017/S0022377800008333 Published online by Cambridge University Press

Finally, it is worth noticing that the type of dissipation, i.e. Γ, does not explicitly show up in (15) in the approximation considered.

5. Dispersion relation

Applying the jump condition (14) to connect the solutions (9) and (10) across the two layers, starting at $x_1 = -(x_0 + \Delta)$ and $x_2 = x_0$ respectively, we obtain the dispersion relations for two groups of eigenmodes *I* and *II* in the considered basic state configuration:

$$\mathscr{D}^{(\mathrm{I},\mathrm{II})} \equiv \mathscr{D}_0^{(\mathrm{I},\mathrm{II})} + \mathscr{D}_1^{(\mathrm{I},\mathrm{II})} = 0, \tag{16}$$

with

$$\mathscr{D}_0^{(\mathrm{I})} \equiv \epsilon_1 \tanh(k_\parallel x_0) + \epsilon_2 + \mathscr{O}(k_\parallel \Delta), \tag{17a}$$

$$\mathscr{D}_1^{(\mathrm{I})} \equiv -ik_\parallel \Delta \epsilon_1 \epsilon_2 \sum_{x_r} \operatorname{sgn} \Im\epsilon(x_r;\omega_0) \left|\frac{\Delta\partial\epsilon}{\partial x}\right|^{-1}_{x=x_r} + \mathscr{O}(k_\parallel^2 \Delta^2) \tag{17b}$$

for the modes *I* and

$$\mathscr{D}_0^{(\mathrm{II})} \equiv \epsilon_1 \coth(k_\parallel x_0) + \epsilon_2 + \mathscr{O}(k_\parallel \Delta), \tag{18a}$$

$$\mathscr{D}_1^{(\mathrm{II})} \equiv -ik_\parallel \Delta \epsilon_1 \epsilon_2 \sum_{x_r} \operatorname{sgn} \Im\epsilon(x_r;\omega_0) \left|\frac{\Delta\partial\epsilon}{\partial x}\right|^{-1}_{x=x_r} + \mathscr{O}(k_\parallel^2 \Delta^2) \tag{18b}$$

for the modes *II*. For each of these two groups of modes, the corresponding dispersion relation (16) has complex solutions

$$\omega = \Re\omega + i\Im\omega \equiv \omega_0 + i\gamma, \qquad \text{where} \quad \frac{\gamma}{\omega_0} = \mathscr{O}(k_\parallel \Delta) \ll 1. \tag{19}$$

The real part of the frequency $\omega_0(k_\parallel)$ defines the frequency spectrum, with accuracy up to small terms $\mathscr{O}(k_\parallel \Delta)$, while the imaginary part $\gamma \ll \omega_0$ determines the damping or growth rate.

6. Frequency spectra

As mentioned above, the eigenfrequency spectra are the real parts of ω obtained from the dispersion relation (16). Neglecting the small terms $\mathscr{O}(k_\parallel \Delta)$ in (16), such eigenfrequencies ω_0 are the solutions of

$$\mathscr{D}_0^{(\mathrm{I},\mathrm{II})}(\omega_0) = 0,$$

which is the dispersion relation for the case $\Delta = 0$ when the boundary layers are replaced by sharp discontinuities. Thus the considered long-wavelength perturbations of the basic state oscillate with frequencies ω_0 unaffected by the finite thickness of the boundary layers, up to small terms of the order of $k_\parallel \Delta$.

6.1. Modes I

According to (4) and (18), the oscillation frequency spectra ω_0 for the modes *I* are solutions of

$$\frac{\Omega_{p1}^2 + \Omega_{p2}^2}{\omega_0^2} + \frac{\omega_{pd2}^2}{(\omega_0 - k_\parallel U_2)^2} - 1 - \tanh(k_\parallel x_0) = 0, \tag{20}$$

https://doi.org/10.1017/S0022377800008333 Published online by Cambridge University Press

where

$$\Omega_1^2 \equiv (\omega_{pe1}^2 + \omega_{pi1}^2)\tanh(k_\parallel x_0) \approx \omega_{pe1}^2 \tanh(k_\parallel x_0),$$
$$\Omega_2^2 \equiv \omega_{pe2}^2 + \omega_{pi2}^2.$$

Here we have taken into account that $\omega_{pe1} \gg \omega_{pi1}$ and also the initial assumption of constant particle density of fully ionized ions throughout the whole system, $\omega_{pi1} = \omega_{pi2} \equiv \omega_{pi}$. As to the particle density of electrons, it could be significantly depleted inside the uniform layer owing to electron attachment to the dust particles and the charge-neutrality condition. For this reason, plasma frequencies of both ions and electrons have to be retained in the expression for Ω_2.

Equation (20) reduces to a fourth-order algebraic equation in ω that can easily be solved, taking into account that the dust component has by far the lowest plasma frequency, i.e. that $\omega_{pd2} \ll \Omega_{1,2}$. In this case, there exist two distinct domains, each containing a pair of solutions to (20) that can readily be obtained in analytical form. The two pairs of solutions will be labelled as the P_I and K_I modes.

6.1.1. Mode P_I. One pair of solutions is obtained if the term containing ω_{pd2} is neglected in (20), which implies that ω_0 is not too close to $k_\parallel U_2$. This then yields real solutions

$$\omega_0 = \pm\left[\frac{\Omega_1^2 + \Omega_2^2}{1 + \tanh(k_\parallel x_0)}\right]^{1/2}, \tag{21}$$

of which only $\omega_0 > 0$ has to be considered. The expression (21) is thus the frequency of a stable plasma surface wave on a layer of streaming dusty plasma, and we shall hence call it the P_I mode. The effect of the flow does not show up, because the small plasma frequency of the moving dust component is negligible in this domain of eigenfrequencies. This, however, does not mean that the overall effect of the dust component is negligible, since its presence appears implicitly through the value of the electron plasma frequency ω_{pe2} which may be reduced even to zero if all electrons are attached to dust particles. In this limiting case, Ω_2 is lowered to ω_{pi}, making the eigenfrequency ω_0 significantly smaller as a result.

6.1.2. Modes $K_I^{(+)}$ and $K_I^{(-)}$. In the case of $\omega_0 \approx k_\parallel U_2$, the term related to the dust component can no longer be neglected in (20) if $k_\parallel U_2 > 0$. We can then substitute ω_0 by $k_\parallel U_2$ into the terms of the electron and ion components, which gives two eigenfrequencies

$$\omega_0 = k_\parallel U_2 \pm k_\parallel U_2 \frac{\omega_{pd2}}{\{[1 + \tanh(k_\parallel x_0)]\, k_\parallel^2 U_2^2 - (\Omega_1^2 + \Omega_2^2)\}^{1/2}}. \tag{22}$$

The solutions with the $\pm$ signs in (22) describe what we shall call convective surface modes $K_I^{(+)}$ and $K_I^{(-)}$ respectively.

We see that a moving dust component introduces two additional modes $K_I^{(+)}$ and $K_I^{(-)}$, which do not exist in the case of a static plasma dust component, when only the P_I mode is present. Moreover, both $K_I^{(+),(-)}$ modes can propagate only in the direction of the flow velocity, in which case $k_\parallel U_2 > 0$. They do not exist if $k_\parallel U_2 < 0$, when only P_I is present.

https://doi.org/10.1017/S0022377800008333 Published online by Cambridge University Press

Another property of the $K_I^{(+),(-)}$ modes is that they may become unstable when the motion of the dust component results in a Buneman-type instability. Namely, as seen from the solution (22), if the product $k_\parallel U_2$ satisfies the instability condition given by

$$k_\parallel^2 U_2^2 \leqslant \frac{\Omega_1^2+\Omega_2^2}{1+\tanh(k_\parallel x_0)}, \tag{23}$$

the frequency ω_0 becomes complex. Its imaginary part is the Buneman instability growth rate $\gamma_B > 0$, which is equal to

$$\gamma_B = k_\parallel U_2 \frac{\omega_{pd2}}{\{(\Omega_1^2+\Omega_2^2)-[1+\tanh(k_\parallel x_0)]\,k_\parallel^2 U_2^2\}^{1/2}},$$

while the real part of the frequency is the convective term $k_\parallel U_2$.

6.2. Modes II

The expressions for the modes *II* are analogous to the modes *I*, and are obtained by replacing $\tanh(k_\parallel x_0)$ with $\coth(k_\parallel x_0)$, as can be seen from (19). Thus we again obtain one mode P_{II} and two additional modes $K_{II}^{(+),(-)}$.

In contrast to the modes *I*, the modes *II* vanish in the limit $k_\parallel x_0 \to 0$. In the other limit, as $k_\parallel x_0 \to \infty$, i.e. when the thickness of the layer is infinite, the modes *I* and *II* coalesce and describe surface waves on a single boundary layer.

7. Resonant processes

As said before, the presence of non-uniform boundary layers on both sides of the dust flow introduces singularities into the equations and allows for local resonant processes within the two layers. Locations where resonances occur are the points $x = x_r$ where $\epsilon(x;\omega)$ vanishes locally at the eigenmode frequency ω_0. The resonant condition given by (7) is then

$$\epsilon(x_r;\omega_0) \equiv 1-\frac{\Omega^2(x_r)}{\omega_0^2}-\frac{\omega_{pd}^2(x_r)}{[\omega_0-k_\parallel U_0(x_r)]^2} = 0, \tag{24}$$

where $\Omega^2(x) \equiv \omega_{pe}^2(x)+\omega_{pi}^2(x)$ can be considered as the local plasma frequency since $\Omega(x) \gg \omega_{pd}(x)$. Owing to this ordering, (24) has two domains of solutions for resonant points that can be easily obtained analytically.

7.1. Plasma resonances

One domain of solutions (24) is for $k_\parallel U_0(x_r)$ not close to the eigenfrequency ω_0, when the term with $\omega_d(x_r)$ can be neglected in (24). This then yields the frequency-matching condition

$$\omega_0 = \Omega(x_r) \quad \text{if } k_\parallel U_0(x_r) \neq \omega_0, \tag{25}$$

which determines the location of the resonant point x_r.

The expression (25) is the condition that the surface eigenmode resonantly excites local plasma oscillations at $x = x_r$, and hence we call it the plasma resonance. The relation (25) can also be understood as the energy conservation law for energy tranfer from surface modes to local plasma oscillations.

https://doi.org/10.1017/S0022377800008333 Published online by Cambridge University Press

7.2. Flow resonances

The second solution to (24) occurs at locations where $k_\parallel U_0(x_r) \approx \omega_0$. In this case, we may neglect the term with $\Omega(x_r)$, and (24) reduces to two resonant conditions

$$\omega_0 = k_\parallel U_0(x_r) + \omega_{pd}(x_r), \tag{26}$$

$$k_\parallel U_0(x_r) = \omega_0 + \omega_{pd}(x_r), \tag{27}$$

indicating a resonant interaction of surface waves with the flow of charged dust particles. We shall refer to these as the flow resonances.

Equation (26) shows that the energy of surface modes is involved in two resonant processes, on the one hand to excite local plasma oscillations of the dust component and on the other hand to increase the kinetic energy of the flow itself. The surface modes are thus losing energy and are damped by this resonance.

Equation (27) indicates a different resonant process, in which energy is transferred from the flow to both surface modes and plasma oscillations of the dust component. In this case, a resonant instability takes place and is independent from the Buneman-type instability described earlier.

8. Growth rates γ

A consequence of resonances in boundary layers is that the eigenfrequency ω becomes complex, as given by (19). The additional imaginary part of ω comes from the term $\mathscr{D}_1$ in the dispersion relation (16) for each of the two modes *I* and *II*. To compute this imaginary part γ, we expand the dispersion function $\mathscr{D}(\omega) \equiv \mathscr{D}_0(\omega) + \mathscr{D}_1(\omega)$ in a power series around ω_0 giving

$$\mathscr{D}_1(\omega_0) + i\gamma \left.\frac{\partial \mathscr{D}_0}{\partial \omega}\right|_{\omega=\omega_0} + \ldots = 0,$$

which yields a general expression for γ as

$$\gamma = -\left.\frac{\Im \mathscr{D}_1}{\dfrac{\partial \mathscr{D}_0}{\partial \omega}}\right|_{\omega=\omega_0}. \tag{28}$$

The derivative of the dissipationless dispersion function $\mathscr{D}_0(\omega)$ can be written as

$$\left.\frac{\partial \mathscr{D}_0}{\partial \omega}\right|_{\omega=\omega_0} = \frac{2(\Omega_1^2 + \Omega_2^2)}{\omega_0^3} + \frac{2\omega_{pd2}^2}{(\omega_0 - k_\parallel U_2)^3}. \tag{29}$$

Depending on whether the sign of γ is positive or negative in (28), we have unstable or damped waves respectively.

To get a better insight into the structure of the growth rate γ, we shall express it in a more explicit way, restricting ourselves to mode *I*, because the conclusions can easily be extrapolated to mode *II* by replacing $\tanh(k_\parallel x_0)$ with $\coth(k_\parallel x_0)$, as already seen before.

Hence (18) gives for mode *I* that

$$\Im \mathscr{D}_1 = \Im \mathscr{D}_1^{(\mathrm{I})} \equiv \pi k_\parallel \epsilon_1^2 \tanh(k_\parallel x_0) \sum_{x_r} \operatorname{sgn} \Im \epsilon(x_r; \omega_0) \left|\frac{\partial \epsilon}{\partial x}\right|^{-1}_{x=x_r}. \tag{30}$$

https://doi.org/10.1017/S0022377800008333 Published online by Cambridge University Press

The summation is taken over all singularities related to the eigenmode of frequency ω_0.

In (30), the sign of $\Im\epsilon(x_r;\omega_0)$ depends on the choice of a particular modal frequency ω_0 and on the resonant condition that it satisfies. It can easily be deduced from the expression for $\epsilon(x_r;\omega_0)$, with dissipations introduced by an imaginary Γ as given by (13):

$$\Im\epsilon(x_r;\omega_0) = 2\Gamma\left\{\frac{\Omega(x_r)^2}{\omega_0^3}+\frac{\omega_{pd}^2(x_r)}{[\omega_0-k_\parallel U_0(x_r)]^3}\right\}. \tag{31}$$

The absolute value of the x derivative of $\epsilon(x;\omega)$ in (30) takes the form

$$\left|\frac{\partial\epsilon}{\partial x}\right| = \left|\frac{1}{\omega_0^2}\frac{d\Omega^2(x)}{dx}+\frac{1}{[\omega_0-k_\parallel U_0(x)]^2}\frac{d\omega_{pd}^2(x)}{dx}+\frac{2k_\parallel}{[\omega_0-k_\parallel U_0(x)]^3}\frac{dU_0(x)}{dx}\right|. \tag{32}$$

The growth rate γ as given by (28) and (30) can be understood as a sum of partial growth rates γ_{x_r} related to contributions of each resonance x_r separately:

$$\gamma = \sum_{x_r}\gamma_{x_r}, \tag{33a}$$

where

$$\gamma_{x_r} \equiv -\pi k_\parallel \epsilon_1^2 \tanh(k_\parallel x_0)\left.\frac{\operatorname{sgn}\Im\epsilon(x_r;\omega_0)}{\left|\dfrac{\partial\epsilon}{\partial x}\right|_{x_r}\dfrac{\partial\mathscr{D}_0}{\partial\omega}}\right|_{\omega_0}. \tag{33b}$$

Now that all the elements in the expression (28) for γ are known, we may study each of the resonant processes separately for the three modes P_I and $K_I^{(+),(-)}$.

8.1. Resonances of the P_I mode

As given by (21), the eigenfrequency ω_0 of the mode P_I is

$$\omega_0^2 = \frac{\omega_{pe1}^2\tanh(k_\parallel x_0)+\omega_{pe2}^2+\omega_{pi2}^2}{1+\tanh(k_\parallel x_0)}, \tag{34}$$

while (29) yields

$$\left.\frac{\partial\mathscr{D}_0}{\partial\omega}\right|_{\omega_0} = 2\frac{\Omega_1^2+\Omega_2^2}{\omega_0^3},$$

with ω_0 given by (34).

The frequency (34) of the P_I mode can satisfy all three resonant conditions (25)–(27), as shown below for each of the three resonances. The growth rate γ then reflects the joint effect of all three resonant processes acting simultaneously.

According to (25), the plasma resonance is achieved at $x = x_r \equiv x_{(p)}$, where

$$\omega_0 = [\omega_{pe}^2(x_{(p)})+\omega_{pi}^2(x_{(p)})]^{1/2}.$$

In this case, (31) and (32) give

$$\Im\epsilon(x_{(p)}) > 0, \qquad \left|\frac{d\epsilon}{dx}\right|_{x_{(p)}} = \left|\frac{d}{dx}\ln\Omega^2\right|_{x_{(p)}}.$$

The flow resonances (26) and (27) too can be satisfied for the eigenfrequency

https://doi.org/10.1017/S0022377800008333 Published online by Cambridge University Press

(34). This occurs at $x = x_r \equiv x_{(+)}$ and $x = x_r \equiv x_{(-)}$ for (26) and (27) respectively, so that (31) and (32) yield

$$\Im\epsilon(x_{(+)}) > 0, \qquad \left|\frac{d\epsilon}{dx}\right|_{x_{(+)}} = \left|\frac{d}{dx}\ln\omega_{pd}^2\right|_{x_{(+)}} \tag{35}$$

for the $f_{(+)}$ resonance given by (26), and

$$\Im\epsilon(x_{(-)}) < 0, \qquad \left|\frac{d\epsilon}{dx}\right|_{x_{(-)}} = \left|\frac{d}{dx}\ln\omega_{pd}^2\right|_{x_{(-)}} \tag{36}$$

for the $f_{(-)}$ resonance given by (27).

The full growth rate γ as expressed in (33) is now the sum of three terms related to the three resonances:

$$\gamma = \gamma_{(p)} + \gamma_{(+)} + \gamma_{(-)}.$$

We see immediately that the contributions of the flow resonances cancel out mutually since $\gamma_{(+)} = -\gamma_{(-)}$, according to (35) and (36). The effect of the surface-wave instability occurring at $x_{(-)}$ with $\gamma_{(-)} > 0$ is thus exactly balanced by the damping at $x_{(+)}$ with $\gamma_{(+)} < 0$. The energy of the flow is being first transferred to the surface mode at $x = x_{(-)}$ and then back to the flow at $x = x_{(+)}$. What remains is the additional wave damping that occurs at the plasma resonance $x = x_{(p)}$ with $\gamma_{(p)} < 0$.

The P_I mode is therefore damped with a negative growth rate (33) that takes the following normalized form:

$$\frac{\gamma}{\omega_0} = \frac{\gamma_{x_{(p)}}}{\omega_0} \equiv -\pi k_\parallel \epsilon_1^2(\omega_0)\tanh(k_\parallel x_0)\frac{\omega_0^2\,\Omega(x_{(p)})}{4[\Omega_1^2(\omega_0)+\Omega_2^2(\omega_0)]\,|\Omega'(x_{(p)})|}, \tag{37}$$

where $\Omega'(x_{(p)}) \equiv d\Omega/dx$ taken at $x = x_{(p)}$ and ω_0 given by (34).

As said before, a replacement of tanh by coth in Ω_1 and in the expression (37) shows that the P_{II} mode is damped in the same way as the P_I mode and has a negative growth rate

$$\frac{\gamma}{\omega_0} = \frac{\gamma_{x_{(p)}}}{\omega_0} \equiv -\pi k_\parallel \epsilon_1^2(\omega_0)\coth(k_\parallel x_0)\frac{\omega_0^2\,\Omega(x_{(p)})}{4[\Omega_1^2(\omega_0)+\Omega_2^2(\omega_0)]\,|\Omega'(x_{(p)})|}.$$

8.2. Resonances of $K_I^{(+)}$ and $K_I^{(-)}$ modes

The eigenfrequencies of the other two modes are both close to $k_\parallel U_2$, since

$$\omega_0 = k_\parallel U_2\left(1 \pm \frac{\omega_{pd2}}{A^{1/2}}\right), \tag{38a}$$

where

$$A \equiv [1+\tanh(k_\parallel x_0)]\,k_\parallel^2 U_2^2 - (\Omega_1^2+\Omega_2^2), \tag{38b}$$

as seen from (22), so that

$$\left.\frac{\partial\mathscr{D}_0}{\partial\omega}\right|_{\omega_0} = \pm\frac{2A^{3/2}}{k_\parallel^3 U_2^3\,\omega_{pd2}}$$

for the $K_I^{(+)}$ and $K_I^{(-)}$ modes respectively. In what follows, we shall assume $A > 0$, i.e. we consider perturbations that are stable to the Buneman-type instability according to the criterion (23).

https://doi.org/10.1017/S0022377800008333 Published online by Cambridge University Press

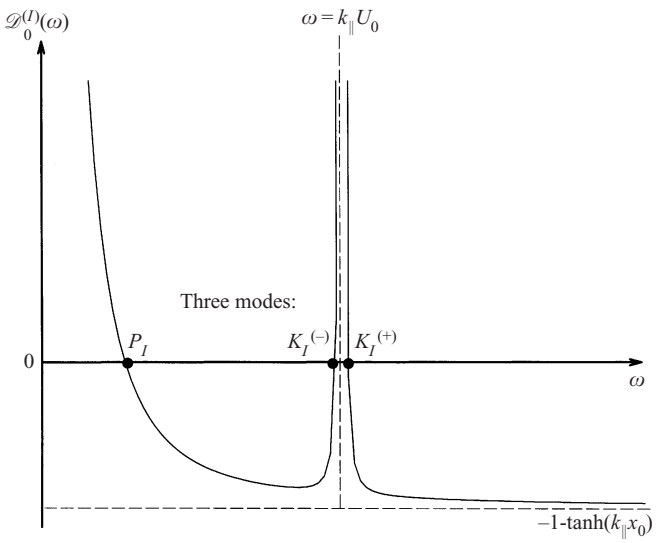


Figure 2. Schematic plot of the dispersion function, showing the three modal frequencies of the P and $K_I^{\pm}$ modes.

The location of the resonant point is expected to be somewhere in the interior of the boundary layers, where the speed of the flow $U_0(x)$ should differ by some positive amount ΔU_0 from its uniform value U_2 in region 2. Consequently,

$$\omega_0 - k_\parallel U_0(x) \approx k_\parallel [U_2 - U_0(x)] \geqslant k_\parallel \Delta U_0 > 0,$$

i.e. the above difference of speeds is positive and not close to zero at any resonant point $x = x_r$. For this reason, only the plasma resonant condition (25) can be satisfied for the $K_I^{(+)}$ and $K_I^{(-)}$ modes, since the term with $\omega_{pd}(x)$ is always negligible in (24). Thus we have two plasma resonances defined by

$$\omega_0 = \Omega(x_r) \pm \mathscr{O}(\omega_{pd}/\omega_0)$$

for the two modes, which are very close together, as shown in Fig. 2. Practically, they occur at the same point at which $\omega_0 = \Omega(x_r)$, where the flow directly resonates with local plasma oscillations.

Equations (31) and (32) now yield the same expressions

$$\Im\epsilon > 0, \qquad \left|\frac{\partial \epsilon}{\partial x}\right| = \left|2\frac{\Omega'(x_r)}{\Omega(x_r)}\right|$$

for both modes, since here $\omega_0^2 \approx \Omega^2(x_r) \approx k_\parallel U_2$.

Finally, the related normalized growth rates are

$$\frac{\gamma_{(+)}}{\omega_0} = -\pi k_\parallel \epsilon_1^2(\omega_0) \tanh(k_\parallel x_0) \frac{\omega_0^2 \omega_{pd2}}{4A^{3/2}} \frac{\Omega(x_r)}{|\Omega'(x_r)|} \tag{39}$$

for the $K_I^{(+)}$ mode, and

$$\frac{\gamma_{(-)}}{\omega_0} = \pi k_\parallel \epsilon_1^2(\omega_0) \tanh(k_\parallel x_0) \frac{\omega_0^2 \omega_{pd2}}{4A^{3/2}} \frac{\Omega(x_r)}{|\Omega'(x_r)|} \tag{40}$$

for the $K_I^{(-)}$ mode.

https://doi.org/10.1017/S0022377800008333 Published online by Cambridge University Press

We see from (39) and (40) that the mode $K_I^{(+)}$, which propagates with a phase velocity slightly bigger than U_2, is damped, while the mode $K_I^{(-)}$, propagating slower than U_2, is unstable. This resonant instability exists when the system is stable to the Buneman instability, i.e. for $A > 0$ in (38) or for $k_\parallel^2 U_2^2$ satisfying the inequality

$$k_\parallel^2 U_2^2 \approx \Omega^2(x_r) > \frac{\Omega_1^2 + \Omega_2^2}{1 + \tanh(k_\parallel x_0)}. \tag{41}$$

9. Conclusions

We have discussed eigenmodes in a dusty plasma, where the dust is confined to a slab, and electron depletion occurs inside this region. Outside, the plasma is just a normal uncontaminated plasma, but between the inside and outside regions there are smooth transition or boundary layers. The presence of dust reduces the electron concentration in the inner region, but the ions have a constant density throughout. In addition, the dust component can flow with respect to the plasma, as a first approximation to cometary tails, where there is a notable difference between the fast flowing solar wind and the slow moving dust tail, viewed in the comet frame.

Since the equilibrium densities and flows are non-uniform, the description involves a space-dependent dielectric function, which then indicates the possibility of singular points, where resonances occur with local plasma oscillations. We have studied surface eigenmodes that are evanescent outside the dust region, and have matched the solutions from the uniform inside and outside regions through the boundary layers on both sides of the dusty plasma region. For sufficiently rapid transitions, analytical solutions are possible, and these give rise to two distinct frequency domains, each of which has pairs of solutions. One of these refers to plasma surface waves, unaffected by the dust flow. The other pair leads to convective surface modes, which become unstable for large flow speeds, akin to Buneman-type instabilities. A detailed study has been made of the resonant processes in the boundary layers, including damping and growth rates.

Of course, the slab model with smooth boundary layers was adopted here for reasons of analytical tractability, but we believe that our work will find application in different astrophysical and space environments. We intend to generalize our detailed approach to magnetized cylindrical geometries, so as to better model cometary tails or flux tubes in space and solar plasmas, where magnetic fields are always present.

Acknowledgements

This work was supported by the Bijzonder Onderzoeksfonds of the Universiteit Gent through a sabbatical visitor grant (V.M.Č.) and a research grant (F.V.).

References

Bharuthram, R. and Shukla, P. K. 1993 Low-frequency surface waves on a warm dusty plasma. *Planet. Space Sci.* **41**, 17–19.

Bliokh, P. V. and Yaroshenko, V. V. 1985 Electrostatic waves in Saturn's rings. *Soviet Astron.* **29**, 330–336.

https://doi.org/10.1017/S0022377800008333 Published online by Cambridge University Press

Bliokh, P., Sinitsin, V. and Yaroshenko, V. 1995 *Dusty and Self-Gravitational Plasmas in Space*. Kluwer, Dordrecht.

Cramer, N. F. and Vladimirov, S. V. 1996 Alfvén surface waves in a magnetized dusty plasma. *Phys. Plasmas* **3**, 4740–4747.

Cramer, N. F., Yeung, L. K. and Vladimirov, S. V. 1998 Surface waves in a magnetized plasma with mobile dust grains. *Phys. Plasmas* **5**, 3126–3134.

Horányi, M. 1996 Charged dust dynamics in the solar system. *Annu. Rev. Astron. Astrophys.* **34**, 383–418.

Kotsarenko, A. N., Kotsarenko, N. Ya. and Silich, S. A. 1998 Low frequency surface waves in the magnetized dusty plasma. *Planet. Space Sci.* **46**, 399–403.

Mendis, D. A. and Rosenberg, M. 1994 Cosmic dusty plasma. *Annu. Rev. Astron. Astrophys.* **32**, 419–463.

Ostrikov, K. N. and Yu, M. Y. 1998 Ion-acoustic surface waves on a dielectric-dusty plasma interface. *IEEE Trans. Plasma Sci.* **26**, 100–103.

Ostrikov, K. N., Vladimirov, S. V. and Yu, M. Y. 1999 Low-frequency surface waves in a structured magnetized dusty plasma. *J. Geophys. Res.* **104**, 593–596.

Rao, N. N., Shukla, P. K. and Yu, M. Y. 1990 Dust-acoustic waves in dusty plasmas. *Planet. Space Sci.* **38**, 543–546.

Shukla, P. K. 1992 Low-frequency modes in dusty plasmas. *Physica Scripta* **45**, 504–507.

Spitzer, L. 1941 The dynamics of the interstellar medium. I. Local equilibrium. *Astrophys. J.* **93**, 369–379.

Verheest, F. 1996 Waves and instabilities in dusty space plasmas. *Space Sci. Rev.* **77**, 267–302.

https://doi.org/10.1017/S0022377800008333 Published online by Cambridge University Press